

# NaZnF<sub>3</sub> as a low-pressure analogue of MgSiO<sub>3</sub>

(Author Accepted Manuscript version)

Dominik Kurzydłowski,<sup>1\*</sup> Arkadiusz Gajek,<sup>2</sup> Zoran Mazej,<sup>3</sup>

<sup>1</sup> Faculty of Mathematics and Natural Sciences, Cardinal Stefan Wyszyński University in Warsaw, 01-038 Warsaw, Poland;

<sup>2</sup> Institute of Physical Chemistry, Polish Academy of Sciences, 01-224 Warsaw, Poland;

<sup>3</sup> Department of Inorganic Chemistry and Technology, Jožef Stefan Institute, SI-1000 Ljubljana, Slovenia

\* [d.kurzydowski@uksw.edu.pl](mailto:d.kurzydowski@uksw.edu.pl)

Solid-state systems whose properties at high pressure (exceeding 1 GPa) mimic those of MgSiO<sub>3</sub> are of large importance in the study of the interior of planets. By means of Density Functional Theory (DFT) calculations we studied the high-pressure properties of a MgSiO<sub>3</sub> analogue, NaZnF<sub>3</sub>. We reproduce the phase-transition sequence previously reported for this compound (GdFeO<sub>3</sub> → CaIrO<sub>3</sub> → La<sub>2</sub>S<sub>3</sub>), and predict that it should undergo a two-step dissociation: decomposition into an equimolar mixture of Na<sub>2</sub>ZnF<sub>4</sub> and NaZn<sub>2</sub>F<sub>5</sub> at 25.4 GPa, followed by a breakdown into ZnF<sub>2</sub> and NaF at 66.8 GPa. These processes are analogous to those predicted for compressed MgSiO<sub>3</sub>. Moreover, both Na<sub>2</sub>ZnF<sub>4</sub> and NaZn<sub>2</sub>F<sub>5</sub> are isostructural with analogous phases from the Mg-Si-O system. We also find that both these novel compounds are thermodynamically stable at ambient conditions (Na<sub>2</sub>ZnF<sub>4</sub>) or at low pressure of 19 GPa (NaZn<sub>2</sub>F<sub>5</sub>). Our study indicates that NaZnF<sub>3</sub> could serve as a good low-pressure analogue of MgSiO<sub>3</sub> exhibiting the same sequence of phase transitions, and pressure induced decomposition, but at pressures an order of magnitude lower.

## I. INTRODUCTION

The perovskite (GdFeO<sub>3</sub>-type) and post-perovskite (CaIrO<sub>3</sub>-type) polymorphs of MgSiO<sub>3</sub> are the major constituents of the Earth's mantle. It is assumed that they are also present in the interior of other rocky planets, including super-Earths. Therefore, modelling the properties of the interior of these objects requires knowledge on the properties of silicates at conditions found there (pressures exceeding 500 GPa) [1]. This knowledge is acquired mainly through laboratory experiments, in most cases utilizing the diamond anvil cell (DAC). The importance of high-pressure experiments is exemplified by the discovery of the perovskite to post-perovskite transition in MgSiO<sub>3</sub> at 125 GPa, which explained the unusual properties of the lowermost part of the Earth's mantle (the D'' layer) [2–4].

Despite the impressive progress in experimental techniques [5–10], recreating the extreme conditions of the interiors of planets in the laboratory is still very challenging. For that reason *ab initio* modelling [11–14], as well as experiments on MgSiO<sub>3</sub> analogs, are often used in the study of the deep Earth [15]. The so-called low-pressure analogs (LPAs) of MgSiO<sub>3</sub> are systems which display similar chemistry, phase transition sequence, and structure-property relations, but at lower pressures (typically below 50 GPa). With the increasing number of newly discovered exoplanets [16], the study on LPAs has gained much attention with several systems proposed as MgSiO<sub>3</sub> analogs, such as NaMgF<sub>3</sub> [17–25], KZnF<sub>3</sub> [26–29], and MgGeO<sub>3</sub> [30–33]. The interest in the high-pressure behavior of LPAs was

mostly focused on the pressure-induced phase transitions in the parent  $ABX_3$  system [34]. However, recent theoretical studies indicated that at pressures exceeding 750 GPa (0.75 TPa) the post-perovskite phase of  $MgSiO_3$  should decompose via a three-step process, with the formation of  $Mg_2SiO_4$  and  $MgSi_2O_5$  in the first step [35–37]. This shifted the focus towards pressure-induced decomposition of  $MgSiO_3$  analogues [24,25].

Here we present a computational investigation, based on solid state Density Functional Theory (DFT), on the ability of  $NaZnF_3$  to exhibit the same phase transition sequence and pressure-induced decomposition as  $MgSiO_3$ , but at much lower pressures. We also analyze the geometry of the thermodynamically stable compositions of this compound at high pressure, and make a comparison between  $NaZnF_3$  and two other recently proposed LPAs,  $NaMgF_3$  and  $MgGeO_3$ .

## II. COMPUTATIONAL METHODS

Periodic DFT calculations of the geometry and enthalpy of high-pressure polymorphs of  $NaF$ ,  $ZnF_2$ ,  $NaZnF_3$ ,  $Na_2ZnF_4$ , and  $NaZn_2F_5$  utilized the PBEsol functional [38], as implemented in CASTEP (version 19.11) [39]. We found that for  $NaZnF_3$  the chosen method yields phase transition pressures, and the pressure dependence of the unit cell vectors in line with experiment – see Fig. S1 and Table S1 in the Supplemental Material [40]. Good agreement between theory and calculations was also found for the Raman spectrum of the ambient-pressure  $GdFeO_3$  structure of  $NaZnF_3$  (Fig. S2) [40].

The valence electrons were described with a plane-wave basis set (1100 eV cut-off), while norm-conserving pseudopotentials were used for the description of core electrons (Na:  $2s^2 2p^6 3s^1$ , F:  $2s^2 2p^5$ , Zn:  $3d^{10} 4s^2$ ). The convergence criterion for the electronic minimization was  $10^{-7}$  eV per atom. Sampling of the Brillouin zone was done through a Monkhorst–Pack mesh [41], with a  $2\pi \times 0.03 \text{ \AA}^{-1}$  spacing of  $k$ -points. Geometry optimization of the crystal structures was performed with the use of the Broyden–Fletcher–Goldfarb–Shanno scheme [42]. Structures were optimized until the following convergence criteria were met: (i) forces acting on the atoms were smaller than  $5 \text{ meV/\AA}$ ; (ii) difference between the applied hydrostatic pressure and all stress components was smaller than 0.05 GPa; (iii) the maximum ionic displacement smaller than  $5 \cdot 10^{-4} \text{ \AA}$ .

Evolutionary algorithm searches were performed to identify the lowest-enthalpy structures of  $NaZnF_3$ ,  $Na_2ZnF_4$ , and  $NaZn_2F_5$  at high pressure (structural data for the relevant phases is given in Table S2 [40]). Searches were performed with the use of the XtalOpt software (version r12) [43], coupled with DFT calculations utilizing the PBEsol functional (conducted in the VASP software) [44,45]. Searches were done at 10, 40, 80 GPa, and 120 GPa for  $Z$  up to 4. For  $NaZn_2F_5$  an additional search at 10 GPa was conducted for  $Z$  up to 8.

We also used CASTEP for calculating the phonon dispersion curves (with a  $2\pi \times 0.05 \text{ \AA}^{-1}$  q-point spacing) using density-functional perturbation theory (DFPT) [46]. We used a fine FFT grid (CASTEP keywords: `grid_scale : 2.5`, `fine_grid_scale : 3.5`) and more restrictive SCF convergence criterion ( $2 \cdot 10^{-10}$  eV). Phonon dispersion curves for the relevant phases at selected pressures are given in Fig. S3 [40].

Thermodynamic stability of various polymorphs of NaF, NaZnF<sub>3</sub>, Na<sub>2</sub>ZnF<sub>4</sub>, and NaZn<sub>2</sub>F<sub>5</sub> was judged by comparing their enthalpy ( $H$ ), and thus the calculated phase transitions pressures formally correspond to  $T = 0$  K at which the Gibbs free energy ( $G = H - S \cdot T$ , where  $S$  is the entropy) is equal to the enthalpy. Phonon dispersion calculations, performed at selected pressures, confirmed the dynamic stability of the studied phases within their thermodynamic stability window, and enabled calculation of the zero-point energy (ZPE) contribution. The inclusion of ZPE does not influence markedly the phase stability of the studied compounds (see Section III). Visualization of all structures was performed with the VESTA software package [47]. For symmetry recognition we used the FINDSYM program [48].

### III. RESULTS AND DISCUSSION

Before we move to the phase transitions and thermodynamic stability of ternary phases in the Na-Zn-F system we address the computational results for the binary fluorides: NaF, ZnF<sub>2</sub>. For the former we predict a phase transition from the NaCl-type (B1) structure to the CsCl-type (B2) polymorph at 23.5 GPa – in close accordance with the experimental value of 27 GPa [49]. At ambient conditions ZnF<sub>2</sub> adopts the TiO<sub>2</sub> (rutile) structure. Upon compression the following sequence of phase transitions is predicted by our calculations: TiO<sub>2</sub>  $\rightarrow$  CaCl<sub>2</sub>  $\rightarrow$  HP-PdF<sub>2</sub>  $\rightarrow$  HP1-AgF<sub>2</sub>  $\rightarrow$  PbCl<sub>2</sub> (cotunnite), with the Zn<sup>2+</sup> coordination increasing from 6 (TiO<sub>2</sub>, CaCl<sub>2</sub>, HP-PdF<sub>2</sub>) through 7 (HP1-AgF<sub>2</sub>) to 9 (PbCl<sub>2</sub>) [50–52]. These results are in good agreement with recent experimental and computational studies on ZnF<sub>2</sub> [52,53].

#### A. NaZnF<sub>3</sub>

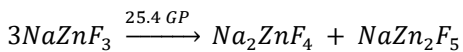
Our calculations also reproduce previous experimental and theoretical results on the high-pressure phase transitions of NaZnF<sub>3</sub> [54–56]. At ambient conditions (effectively 0 GPa) we find the distorted perovskite GdFeO<sub>3</sub>-type structure ( $Pnma$  symmetry) as the most stable polymorph of NaZnF<sub>3</sub> (Fig. 1) – in line with experiment. This structure exhibits octahedral coordination of Zn<sup>2+</sup> by F<sup>-</sup> anions; the coordination number (CN) of Na<sup>+</sup> is 8. The GdFeO<sub>3</sub> structure is predicted to transform to a post-perovskite (CaIrO<sub>3</sub>-type,  $Cmcm$  symmetry) polymorph at 7.7 GPa, in close accordance to the experimental value of 5 GPa (at room temperature) [55]. The CaIrO<sub>3</sub> structure exhibits the same CNs

of the cations as GdFeO<sub>3</sub>, but differs in the connectivity of their coordination polyhedral. In GdFeO<sub>3</sub> each ZnF<sub>6</sub> octahedra shares all of its corners with one neighbor thus forming a 3D network, while in CaIrO<sub>3</sub> corner and edge sharing leads to a layered network [Fig. 2(a)]. We find that CaIrO<sub>3</sub> is dynamically stable even at 1 atm [40] – in accordance with the observed metastability of this polymorph upon pressure quenching [55].

At 23.4 GPa the CaIrO<sub>3</sub> phase is predicted to transform to a La<sub>2</sub>S<sub>3</sub>-type structure (*Pnma* symmetry). This structure, sometimes referred to as Gd<sub>2</sub>S<sub>3</sub>-type, was recently proposed as a post-post-perovskite phase in many ABO<sub>3</sub>, ABF<sub>3</sub>, and A<sub>2</sub>O<sub>3</sub> compounds [34], including NaZnF<sub>3</sub> [56]. At 23.4 GPa the La<sub>2</sub>S<sub>3</sub> polymorph exhibits CN(Zn) and CN(Na) equal to 6 and 8, respectively. However, the coordination environment of Zn<sup>2+</sup> is distorted from the octahedron [Fig. 2(b)]. Pairs of these distorted octahedrons are arranged into 1D chains running along the *b* axis. Upon compression an additional F<sup>-</sup> anion enters the coordination sphere of Zn<sup>2+</sup>, resulting in a change of the coordination polyhedron from a distorted octahedron to a distorted mono-capped trigonal prism (CN = 7). At the same time the coordination number of Na<sup>+</sup> increases to 9. This pressure-induced evolution of the coordination sphere of Zn<sup>2+</sup> mimics that occurring in the HP1-AgF<sub>2</sub>-type high-pressure polymorph of ZnF<sub>2</sub> [52]. The seven-fold coordination of Zn<sup>2+</sup> persists in the La<sub>2</sub>S<sub>3</sub> structure up to 100 GPa, and this polymorph remains the ground-state structure of NaZnF<sub>3</sub> up to that pressure.

High-pressure experiments indicated that above 25 GPa the CaIrO<sub>3</sub> polymorph of NaZnF<sub>3</sub> transforms reversibly into a novel, unidentified phase [54]. Based on DFT calculations Cheng *et al.* proposed that this new phase should be isostructural to Sb<sub>2</sub>S<sub>3</sub> (sometimes referred to as the U<sub>2</sub>S<sub>3</sub>-type structure, *Pnma* space group) which they call *pPv-Pnma* [56]. However, they find that this structure has a higher enthalpy than the La<sub>2</sub>S<sub>3</sub> phase (termed by them *ppPv-Pnma*) in the relevant pressure range. As can be seen in Fig. 1 our calculations confirm this finding.

Just above the CaIrO<sub>3</sub> – La<sub>2</sub>S<sub>3</sub> phase transition, at 25.4 GPa, NaZnF<sub>3</sub> is predicted to become thermodynamically unstable with respect to an equimolar mixture of Na<sub>2</sub>ZnF<sub>4</sub> and NaZn<sub>2</sub>F<sub>5</sub> (Fig. 1):



One may view Na<sub>2</sub>ZnF<sub>4</sub> as NaF-rich, and NaZn<sub>2</sub>F<sub>5</sub> as ZnF<sub>2</sub>-rich with respect to NaZnF<sub>3</sub>. An analogous decomposition path (yielding Mg<sub>2</sub>SiO<sub>4</sub> and MgSi<sub>2</sub>O<sub>5</sub>) is predicted to occur in MgSiO<sub>3</sub> at 750 GPa [37]. As we will show below the decomposition products of NaZnF<sub>3</sub> are predicted to be isostructural with

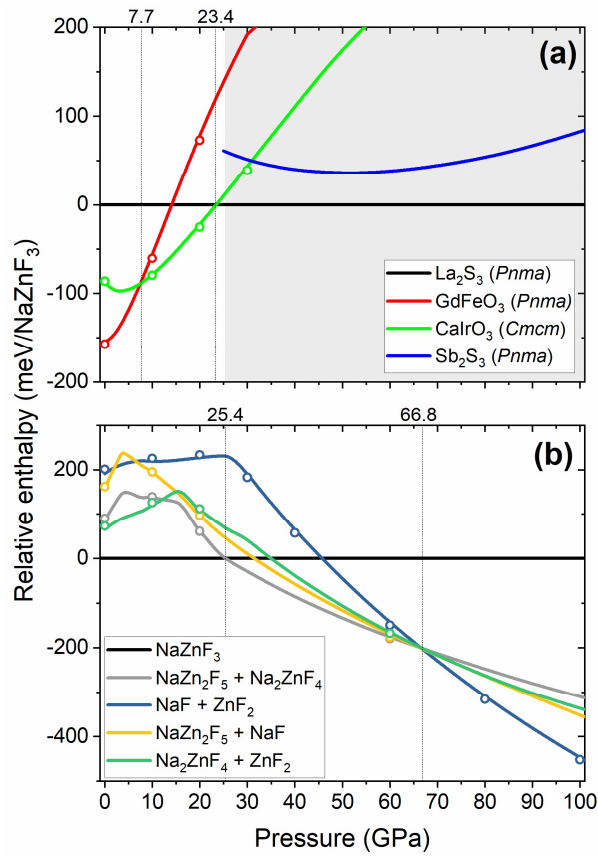


**FIG. 1** (a) Pressure dependence of the relative enthalpy of  $\text{NaZnF}_3$  polymorphs with respect to the enthalpy of the  $\text{La}_2\text{S}_3$  structure (grey area depicts the region in which  $\text{NaZnF}_3$  is thermodynamically unstable); (b) relative enthalpy of  $\text{NaZnF}_3$  dissociation products (within their most stable phases) with respect to  $\text{NaZnF}_3$ . In both (a) and (b) dots indicate ZPE-corrected values. Vertical lines in (a) indicate phase transition of  $\text{NaZnF}_3$  (at 7.7 and 23.4 GPa); vertical lines in (b) indicate the pressure of decomposition of  $\text{NaZnF}_3$  into  $\text{Na}_2\text{ZnF}_4$  and  $\text{NaZn}_2\text{F}_5$  (25.4 GPa), and the subsequent decomposition of these two compounds into  $\text{NaF}$  and  $\text{ZnF}_2$  (at 66.8 GPa)

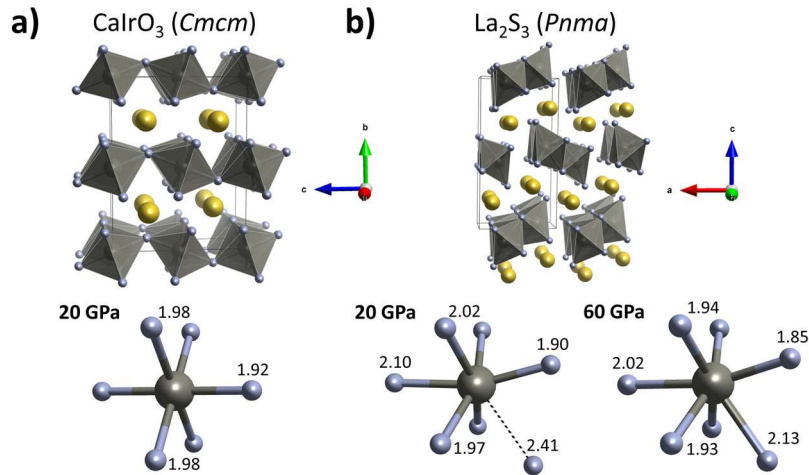
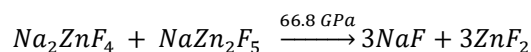


**FIG. 2** The (a)  $\text{CaIrO}_3$  and (b)  $\text{La}_2\text{S}_3$  polymorphs of  $\text{NaZnF}_3$ . Yellow/grey/blue balls denote Na/Zn/F atoms. Atomic distances within the Zn polyhedron at selected pressures are given in Å.

the analogous products of MgSiO<sub>3</sub> decomposition. Upon compression another decomposition event is predicted to occur at 66.8 GPa with both Na<sub>2</sub>ZnF<sub>4</sub> and NaZn<sub>2</sub>F<sub>5</sub> fragmenting into binary fluorides:



At this pressure NaF is predicted to adopt the CsCl-type structure, while ZnF<sub>2</sub> the PbCl<sub>2</sub>-type structure.

## B. Na<sub>2</sub>ZnF<sub>4</sub>

Our calculations indicate that Na<sub>2</sub>ZnF<sub>4</sub>, which although hypothesized has not been reported up to date [57], should be thermodynamically stable even at ambient conditions (Fig. 3). At pressures below 15.6 GPa it is predicted to adopt the Sr<sub>2</sub>PbO<sub>4</sub>-type structure of *Pnma* symmetry which consists of chains built from edge-sharing ZnF<sub>6</sub> octahedra separated by Na<sup>+</sup> cations [Fig. 4(a)]. According to the ICSD database [58], the Sr<sub>2</sub>PbO<sub>4</sub> structure type, together with its lower-symmetry variant (Na<sub>2</sub>CuF<sub>4</sub>-type of *P2<sub>1</sub>/c* symmetry), is adopted at ambient conditions by a range of ternary oxides, but only seven ternary halogens (among them: Na<sub>2</sub>MgCl<sub>4</sub> [59], β-K<sub>2</sub>AgF<sub>4</sub> [60], and Na<sub>2</sub>CuF<sub>4</sub> [61]). It can be viewed as a post-perovskite phase of the layered perovskite K<sub>2</sub>NiF<sub>4</sub>-type structure (*n* = 1 member of the Ruddlesden-Popper series) [62]. At 1 atm the energy of the Sr<sub>2</sub>PbO<sub>4</sub> structure is about 260 meV per Na<sub>2</sub>ZnF<sub>4</sub> (= 25 kJ/mol) lower than that of the spinel structure (*Fd $\bar{3}m$* , *Z* = 8) featuring tetrahedrally coordinated Zn<sup>2+</sup> cations, in accordance with the preference of Zn<sup>2+</sup> to adopt octahedral coordination at ambient pressure.

However, the Sr<sub>2</sub>PbO<sub>4</sub> structure is predicted to transform at 15.6 GPa into a structure of *I $\bar{4}2d$*  symmetry which can be viewed as a distorted variant of the CdMn<sub>2</sub>O<sub>4</sub> spinel [63]. This phase change is connected with a reduction of the CN of Zn<sup>2+</sup> from 8 to 4 [Fig. 4(b)], while the CN of Na<sup>+</sup> increases from 7 to 8. In the *I $\bar{4}2d$*  structure each Zn<sup>2+</sup> cation is surrounded by four F<sup>-</sup> anions forming a distorted tetrahedron (Zn-F distances of 1.96 Å at 15 GPa). Next-nearest-neighbor contacts, also forming a tetrahedron around Zn<sup>2+</sup>, are more than 20 % longer. At 15 GPa the *I $\bar{4}2d$*  structure is analogous to the predicted high-pressure phase of Ag<sub>3</sub>F<sub>4</sub> (=Ag<sup>(I)</sup><sub>2</sub>Ag<sup>(II)</sup>F<sub>4</sub>) [64].

The 4-fold coordination evolves into an 8-fold (4+4) one with pressure, as compression induces a substantial shortening of the next-nearest-neighbor Zn-F contacts – at 100 GPa their length is only 10 % larger than that of the nearest-neighbor contacts [Fig 4(b)]. This increase in the CN of Zn<sup>2+</sup> makes this phase analogous to the *I $\bar{4}2d$*  structure of Mg<sub>2</sub>SiO<sub>4</sub> [37,65,66], where a similar 4+4 coordination (with a similar difference in Mg-O lengths) is found at 1 TPa [37]. For a more detailed comparison of the Na<sub>2</sub>ZnF<sub>4</sub> and Mg<sub>2</sub>SiO<sub>4</sub> structures see the Supplemental Material [40].

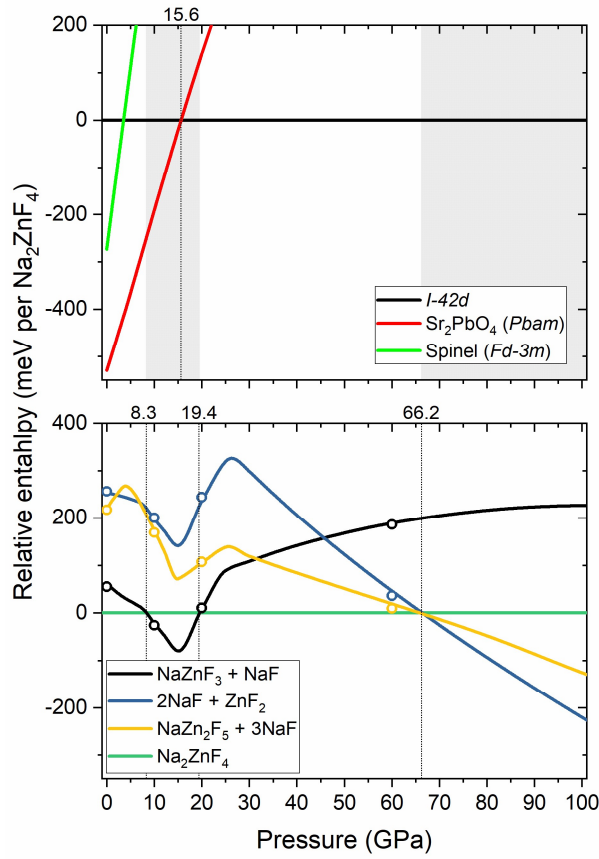


**FIG. 3** (a) Pressure dependence of the relative enthalpy of  $\text{Na}_2\text{ZnF}_4$  polymorphs with respect to the enthalpy of the  $I\bar{4}2d$  structure (grey area depicts the region in which  $\text{Na}_2\text{ZnF}_4$  is thermodynamically unstable); (b) relative enthalpy of  $\text{Na}_2\text{ZnF}_4$  dissociation products (within their most stable phases) with respect to  $\text{Na}_2\text{ZnF}_4$ . In both (a) and (b) dots indicate ZPE-corrected values. The vertical line in (a) indicates the phase transition in  $\text{Na}_2\text{ZnF}_4$  at 15.6 GPa; vertical lines in (b) indicate the pressure of decomposition of  $\text{Na}_2\text{ZnF}_4$  into  $\text{NaZnF}_3$  and  $\text{NaF}$  (8.3 GPa), it's subsequent re-emergence from this mixture (19.4 GPa) and decomposition into  $\text{NaF}$  and  $\text{ZnF}_2$  (at 66.2 GPa).

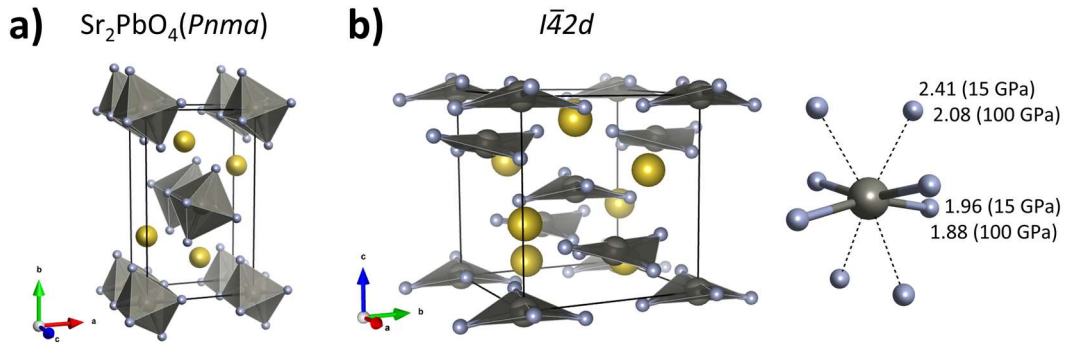
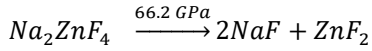


**FIG. 4** The (a)  $\text{Sr}_2\text{PbO}_4$  and (b)  $I\bar{4}2d$  polymorphs of  $\text{Na}_2\text{ZnF}_4$ . Nearest-neighbor and next-nearest-neighbor Zn-F distances in the  $I\bar{4}2d$  structure at 15 and 100 GPa are given in Å. For clarity the unit cell of the  $I\bar{4}2d$  polymorph was shifted by  $(0,0, \frac{1}{2})$ .

Our calculations indicate that at 8.3 GPa  $\text{Na}_2\text{ZnF}_4$  in the  $\text{Sr}_2\text{PbO}_4$  structure should become thermodynamically unstable with respect to decomposition into  $\text{NaZnF}_3$  ( $\text{CaIrO}_3$ -type) and  $\text{NaF}$  ( $\text{CsCl}$ -type).

However, after the  $\text{Sr}_2\text{PbO}_4 \rightarrow I\bar{4}2d$  phase transition  $\text{Na}_2\text{ZnF}_4$  regains its thermodynamic stability at 19.4 GPa. Finally, it is predicted to decompose into binary fluorides ( $\text{NaF} - \text{NaCl}$ ,  $\text{ZnF}_2 - \text{PbCl}_2$ ) at 66.2 GPa, in analogy to what was found for the  $\text{NaZnF}_3$  system:



In order to verify experimentally whether  $\text{Na}_2\text{ZnF}_4$  could be obtained at ambient pressure we have performed a solid-state high-temperature reaction between  $\text{ZnF}_2$  and  $\text{NaF}$  in a 1:2 mole ratio. This did not lead to formation of  $\text{Na}_2\text{ZnF}_4$  – the obtained product was  $\text{NaZnF}_3$  in the  $\text{GdFeO}_3$ -type structure accompanied by excess  $\text{NaF}$  (see Fig. S4 [40]). The discrepancy between this result and the theoretical prediction might lie in temperature effects. However modelling those, for example with the use of the quasi-harmonic approximation [67], lies beyond the scope of the current manuscript.

### C. $\text{NaZn}_2\text{F}_5$

Calculations indicate that  $\text{NaZn}_2\text{F}_5$  is thermodynamically stable between 18.6 and 66.7 GPa (Fig. 5). Below 18.6 GPa this compound is predicted to decompose into  $\text{NaZnF}_3$  ( $\text{CaIrO}_3$ ) and  $\text{ZnF}_2$  (HP- $\text{PdF}_2$ ), above 66.7 GPa it should dissociate into binaries ( $\text{NaF} - \text{B}_2$ ,  $\text{ZnF}_2 - \text{PbCl}_2$ ), as was the case for  $\text{NaZnF}_3$  and  $\text{Na}_2\text{ZnF}_4$ .

In its thermodynamic stability window  $\text{NaZn}_2\text{F}_5$  should adopt a  $P2_1/c$  ( $Z = 4$ ) structure featuring  $\text{Zn}^{2+}$  cations in two coordination environments: distorted square antiprism ( $\text{CN} = 8$ ) and distorted octahedron ( $\text{CN} = 6$ ), as shown in Fig. 6. Upon compression the coordination number of the latter site increases to 7, in analogy to what was found for the  $\text{La}_2\text{S}_3$  phase of  $\text{NaZnF}_3$ . Both at low and high pressure  $\text{Na}^+$  is 9-fold coordinated in the  $P2_1/c$  structure. This polymorph of  $\text{NaZn}_2\text{F}_5$  is isostructural to the predicted ground state structure of  $\text{MgSi}_2\text{O}_5$  [36].

At low pressure the  $P2_1/c$  structure is dynamically stable down to 10 GPa. At this pressure a phonon instability develops at  $Z$  point, that is the  $(\frac{1}{2}, 0, 0)$  wavevector. The distortion resulting from this instability leads to formation of a structure with a doubled unit cell ( $Z = 8$ ) of  $Pnma$  symmetry. This polymorph can be related to  $P2_1/c$  via rotations of the  $\text{Zn}^{2+}$  polyhedra around the  $\mathbf{b}$  cell vector. The  $Pnma$  structure is dynamically stable at ambient pressure hinting at the possibility of quenching to 1 atm  $\text{NaZn}_2\text{F}_5$  synthesized at high pressure.

Despite the fact that at 1 atm  $\text{NaZn}_2\text{F}_5$  is unstable against decomposition into  $\text{NaZnF}_3$  and  $\text{ZnF}_2$ , the enthalpy change associated with the formation of this compound from a 1:2 mixture of  $\text{NaF}$  and  $\text{ZnF}_2$  at this pressure is slightly negative ( $-7.5$  kJ/mol). Therefore we have made an attempt to perform the synthesis of  $\text{NaZn}_2\text{F}_5$  from  $\text{NaF}$  and  $\text{ZnF}_2$  in a 1:2 mole ratio. However, this resulted in the formation

of  $\text{NaZnF}_3$  and excess  $\text{ZnF}_2$  (Fig. S4 [40]), in accordance with the predicted thermodynamics. It seems that a high-pressure synthesis ( $p > 20$  GPa) is required for obtaining  $\text{NaZn}_2\text{F}_5$ .

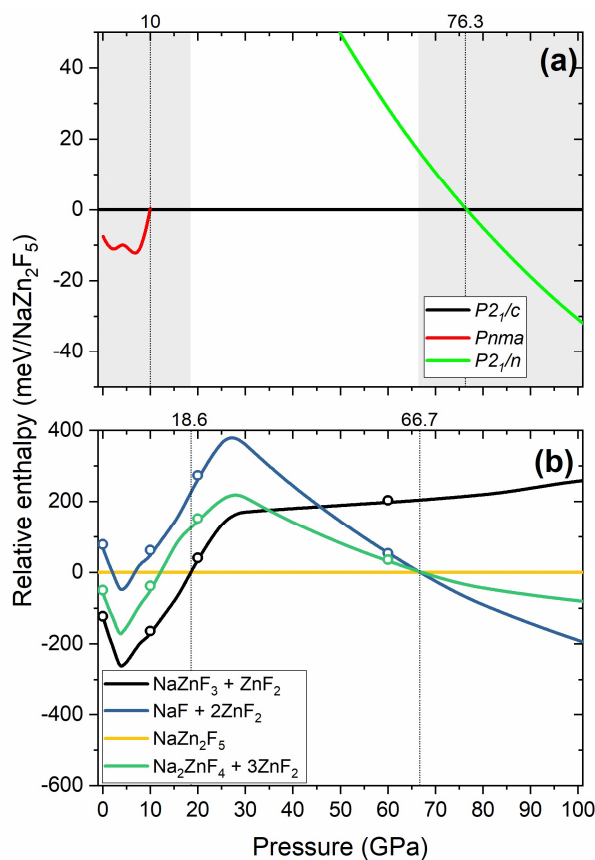


**FIG. 5** (a) Pressure dependence of the relative enthalpy of  $\text{NaZn}_2\text{F}_5$  polymorphs with respect to the enthalpy of the  $P2_1/c$  structure (grey area depicts the region in which  $\text{NaZn}_2\text{F}_5$  is thermodynamically unstable); (b) relative enthalpy of  $\text{NaZn}_2\text{F}_5$  dissociation products (within their most stable phases) with respect to  $\text{NaZn}_2\text{F}_5$ . In (b) dots indicate ZPE-corrected values. The vertical lines in (a) indicates the phase transition in  $\text{NaZn}_2\text{F}_5$  at 10 and 76.3 GPa; vertical lines in (b) indicate the pressure of formation of  $\text{Na}_2\text{ZnF}_4$  from  $\text{NaZnF}_3$  and  $\text{ZnF}_2$  (18.6 GPa), and its decomposition into  $\text{NaF}$  and  $\text{ZnF}_2$  (at 66.7 GPa)

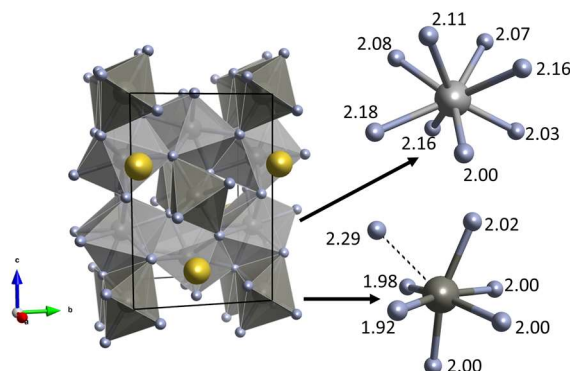
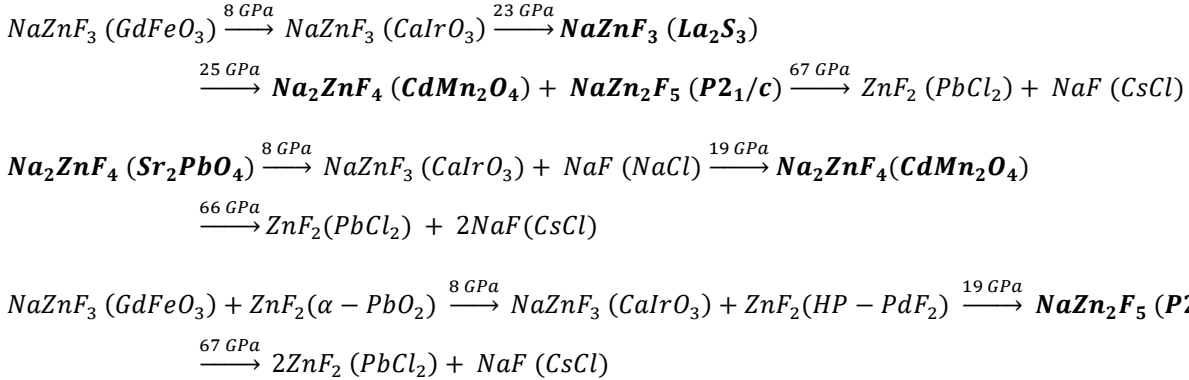


**FIG. 6** The  $P2_1/c$  structure of  $\text{NaZn}_2\text{F}_5$ . Different shades of grey indicate different Zn sites; Zn-F distances at 20 GPa are given in Å.

To summarize the presented results below we give the summary of the ground-state phase transition in the  $\text{NaZnF}_3$ ,  $\text{Na}_2\text{ZnF}_4$ , and  $\text{NaZn}_2\text{F}_5$  systems. Phases that up to date have not been obtained experimentally are given in bolded font.



The general picture that emerges from the our calculations is that at low pressures ( $< 20$  GPa)  $\text{NaZnF}_3$  in its perovskite and post-perovskite structure is the dominant compound in the Na-Zn-F system. Above that pressure NaF-rich ( $\text{Na}_2\text{ZnF}_4$ ) and  $\text{ZnF}_2$ -rich ( $\text{NaZn}_2\text{F}_5$ ) variants emerge as the most stable phases. Above 65 GPa they are predicted to decompose into binary fluorides. Inspection of the equation of states of the most stable phases in each of the three studied systems (Fig. S5 [40]) indicates that the driving force for these transitions is volume reduction. This is also connected with the increase of the coordination number of  $\text{Zn}^{2+}$ : the maximum value found for  $\text{NaZnF}_3$  structure is 7, followed by 8 found for  $\text{Na}_2\text{ZnF}_4$  and  $\text{NaZn}_2\text{F}_5$ , while for  $\text{ZnF}_2$  in the  $\text{PbCl}_2$  structure this value increases to 9. The coordination number of  $\text{Na}^+$  (8) is the same in almost all of the compounds of the Na-Zn-F system.

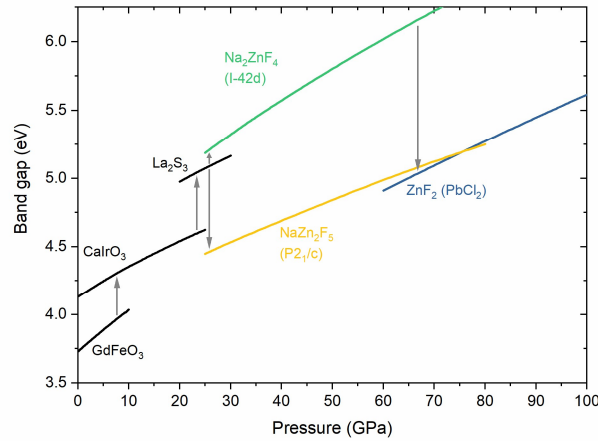


**FIG. 7** The pressure dependence of the band gap on  $\text{NaZnF}_3$  phases,  $\text{Na}_2\text{ZnF}_4$ ,  $\text{NaZn}_2\text{F}_5$ , and  $\text{ZnF}_2$  (black, green, yellow, blue line, respectively). Arrows indicate band gap changes upon phase transitions and decomposition reactions.

Our calculations indicate that all of the members of the Na-Zn-F system are insulating at ambient and high pressure. For all Zn-bearing compounds the electronic band gap increases upon compression (Fig. 7). The rate of this increases is larger for  $\text{NaZnF}_3$  phases and  $I\bar{4}2d$   $\text{Na}_2\text{ZnF}_4$  (0.02 – 0.03 eV/GPa)

compared to  $\text{ZnF}_2$ -rich stoichiometries,  $P2_1/c$   $\text{NaZn}_2\text{F}_5$  and  $\text{PbCl}_2$ -type  $\text{ZnF}_2$  (0.015 eV/GPa). While consecutive phase transition in  $\text{NaZnF}_3$  and formation of  $\text{Na}_2\text{ZnF}_4$  are connected with widening of the band gap, the opposite effect is seen for  $\text{NaZn}_2\text{F}_5$  and  $\text{ZnF}_2$  formation upon  $\text{NaZnF}_3$  decomposition. We note that although the PBEsol functional underestimates the electronic band gap of  $\text{ZnF}_2$ , it models its pressure dependence similarly to more accurate meta-GGA functionals [52,68].

**TABLE I** Summary of the predicted pressures (in GPa) of the perovskite to post-perovskite and post-perovskite to post-post-perovskite phase transitions, as well as the decomposition of  $\text{ABX}_3$  systems. The structure type of the post-post-perovskite phase ( $\text{La}_2\text{S}_3$  or  $\text{Sb}_2\text{S}_3$ ), as well as the type of decomposition products ( $\text{AX}$ ,  $\text{BX}_2$ ,  $\text{A}_2\text{BX}_4$ ,  $\text{AB}_2\text{X}_5$ ) are given in parenthesis. Data for  $\text{MgSiO}_3$ ,  $\text{MgGeO}_3$ ,  $\text{NaMgF}_3$  comes from local density approximation (LDA) calculations [25], results for  $\text{NaZnF}_3$  are from PBEsol calculations (this work).

$\text{ABX}_3$ compound	$\text{GdFeO}_3 \rightarrow \text{CaIrO}_3$	$\text{CaIrO}_3 \rightarrow \text{La}_2\text{S}_3/\text{Sb}_2\text{S}_3$	Decomposition
$\text{MgSiO}_3$	80	1 300 ( $\text{La}_2\text{S}_3$ )	750 ( $\text{A}_2\text{BX}_4 + \text{AB}_2\text{X}_5$ )
$\text{MgGeO}_3$	–	268 ( $\text{La}_2\text{S}_3$ )	178 ( $\text{A}_2\text{BX}_4 + \text{BX}_2$ )
$\text{NaMgF}_3$	18	43 ( $\text{Sb}_2\text{S}_3$ )	29 ( $\text{AX} + \text{AB}_2\text{X}_5$ )
$\text{NaZnF}_3$	8	23 ( $\text{La}_2\text{S}_3$ )	26 ( $\text{A}_2\text{BX}_4 + \text{AB}_2\text{X}_5$ )

As can be seen in Table I,  $\text{NaZnF}_3$  undergoes the same phase transition sequence as  $\text{MgSiO}_3$ , but at much lower pressures. Moreover, it also undergoes the same compression-induced decomposition with the formation of  $\text{A}_2\text{BX}_4$  in the  $I\bar{4}2d$  structure and  $\text{AB}_2\text{X}_5$  in the  $P2_1/c$  structure. In terms of high-pressure behavior  $\text{NaZnF}_3$  is more similar to  $\text{MgSiO}_3$  than other previously proposed LPAs:  $\text{MgGeO}_3$  and  $\text{NaMgF}_3$ . The former system exhibits the  $\text{CaIrO}_3 \rightarrow \text{La}_2\text{S}_3$  phase transition at much higher pressure than  $\text{NaZnF}_3$ , and does not form  $\text{MgGe}_2\text{O}_5$  upon decomposition. In  $\text{NaMgF}_3$  the  $\text{CaIrO}_3$  structure transforms to a  $\text{Sb}_2\text{S}_3$  polymorph, and  $\text{Na}_2\text{MgF}_4$  is not formed upon pressure-induced decomposition. The low pressures of phase transition/decomposition reactions predicted for  $\text{NaZnF}_3$  might facilitate performing high-pressure and high-temperature experiments, which is important in the context of potential large activation barriers associated with the predicted transitions [69]. Exploration of the such barriers in the Na-Zn-F system, although of considerable interest, is beyond the scope of this study.

#### IV. CONCLUSIONS

Our DFT calculations indicate that  $\text{NaZnF}_3$  could serve as a good low-pressure analogue of  $\text{MgSiO}_3$  exhibiting the same sequence of phase transitions, and pressure induced decomposition, but at pressures an order of magnitude lower. All of the structures and compositions stabilized by high pressure in the Na-Zn-F system are analogous to those predicted for Mg-Si-O. We predict that two novel compounds:  $\text{Na}_2\text{ZnF}_4$  and  $\text{NaZn}_2\text{F}_5$  can be obtained at ambient pressure ( $\text{Na}_2\text{ZnF}_4$ ) or relatively low pressure of 19 GPa ( $\text{NaZn}_2\text{F}_5$ ). We note that the latter compound is rare example of a  $\text{AM}_2\text{F}_5$  (A

= alkali metal; M = M<sup>2+</sup>) fluoride – such a composition is only found for M = Sn [70,71], Be [72], Pd [73,74], and Cu [75].

Given the relatively low pressures of the predicted phase transitions and decomposition reaction we hope for a fast experimental verification of the current results. We note, that Raman scattering experiments seem to be a good tool for exploring the high-pressure behavior of this system, as there are considerable differences in the Raman spectrum of Na-Zn-F phases (Fig. S6 [40]). Given that the ambient-pressure high-temperature approach was unsuccessful in the synthesis of Na<sub>2</sub>ZnF<sub>4</sub> and NaZn<sub>2</sub>F<sub>5</sub>, other routes, such as mechanochemical synthesis by using high-energy ball milling (as applied in the case of Zn(BF<sub>4</sub>)<sub>2</sub> synthesis) [76], or high-pressure high-temperature synthesis, with the use of a multi-anvil apparatus [77], might be pursued.

## ACKNOWLEDGEMENTS

D.K. acknowledges the support from the National Science Centre, Poland (NCN) within the SONATA BIS grant (no. UMO-2019/34/E/ST4/00445). This research was carried out with the support of the Interdisciplinary Centre for Mathematical and Computational Modelling at the University of Warsaw (ICM UW), under grant no. GA83-26. Z.M. gratefully acknowledges the financial support from the Slovenian Research Agency (research core funding No. P1-0045 Inorganic Chemistry and Technology).

For the purpose of Open Access, the author has applied a CC-BY public copyright license to any Author Accepted Manuscript (AAM) version arising from this submission.

## REFERENCES

- [1] C. T. Unterborn and W. R. Panero, *The Pressure and Temperature Limits of Likely Rocky Exoplanets*, J. Geophys. Res. Planets **124**, 1704 (2019).
- [2] M. Murakami, K. Hirose, K. Kawamura, N. Sata, and Y. Ohishi, *Post-Perovskite Phase Transition in MgSiO<sub>3</sub>*, Science **304**, 855 (2004).
- [3] A. R. Oganov and S. Ono, *Theoretical and Experimental Evidence for a Post-Perovskite Phase of MgSiO<sub>3</sub> in Earth's D" Layer*, Nature **430**, 445 (2004).
- [4] T. Iitaka, K. Hirose, K. Kawamura, and M. Murakami, *The Elasticity of the MgSiO<sub>3</sub> Post-Perovskite Phase in the Earth's Lowermost Mantle*, Nature **430**, 442 (2004).
- [5] L. Dubrovinsky, N. Dubrovinskaia, V. B. Prakapenka, and A. M. Abakumov, *Implementation*

- of Micro-Ball Nanodiamond Anvils for High-Pressure Studies above 6 Mbar.*, Nat. Commun. **3**, 1163 (2012).
- [6] G. Shen and H. K. Mao, *High-Pressure Studies with x-Rays Using Diamond Anvil Cells*, Reports Prog. Phys. **80**, 016101 (2017).
- [7] A. Dewaele, P. Loubeyre, F. Occelli, O. Marie, and M. Mezouar, *Toroidal Diamond Anvil Cell for Detailed Measurements under Extreme Static Pressures*, Nat. Commun. **9**, 2913 (2018).
- [8] F. Jin, Y. Yang, A.-M. Zhang, J.-T. Ji, and Q.-M. Zhang, *Raman Scattering under Extreme Conditions*, Chinese Phys. B **27**, 077801 (2018).
- [9] S. Hsieh, P. Bhattacharyya, C. Zu, T. Mittiga, T. J. Smart, F. Machado, B. Kobrin, T. O. Höhn, N. Z. Rui, M. Kamrani, S. Chatterjee, S. Choi, M. Zaletel, V. V. Struzhkin, J. E. Moore, V. I. Levitas, R. Jeanloz, and N. Y. Yao, *Imaging Stress and Magnetism at High Pressures Using a Nanoscale Quantum Sensor*, Science (80-. ). **366**, 1349 (2019).
- [10] N. Holtgrewe, E. Greenberg, C. Prescher, V. B. Prakapenka, and A. F. Goncharov, *Advanced Integrated Optical Spectroscopy System for Diamond Anvil Cell Studies at GSECARS*, High Press. Res. **39**, 457 (2019).
- [11] R. M. Wentzcovitch, J. L. Martins, and G. D. Price, *Ab Initio Molecular Dynamics with Variable Cell Shape: Application to MgSiO<sub>3</sub>*, Phys. Rev. Lett. **70**, 3947 (1993).
- [12] F. González-Cataldo, F. Soubiran, H. Peterson, and B. Militzer, *Path Integral Monte Carlo and Density Functional Molecular Dynamics Simulations of Warm Dense MgSiO<sub>3</sub>*, Phys. Rev. B **101**, 024107 (2020).
- [13] Z. Zhang and R. M. Wentzcovitch, *Ab Initio Lattice Thermal Conductivity of MgSiO<sub>3</sub> across the Perovskite-Postperovskite Phase Transition*, Phys. Rev. B **103**, 144103 (2021).
- [14] Z. Zhang and R. M. Wentzcovitch, *Ab Initio Anharmonic Thermodynamic Properties of Cubic CaSiO<sub>3</sub> Perovskite*, Phys. Rev. B **103**, 104108 (2021).
- [15] S. A. T. Redfern, *Using Mineral Analogs to Understand the Deep Earth*, in *Deep Earth: Physics and Chemistry of the Lower Mantle and Core* (2016), edited by H. Terasaki and R.A. Fischer (Wiley, New York, 2016) pp. 101–110.
- [16] B. J. S. Pope, M. Bedell, J. R. Callingham, H. K. Vedantham, I. A. G. Snellen, A. M. Price-Whelan, and T. W. Shimwell, *No Massive Companion to the Coherent Radio-Emitting M Dwarf GJ 1151*, Astrophys. J. **890**, L19 (2020).

- [17] C. D. Martin, W. A. Crichton, H. Liu, V. Prakapenka, J. Chen, and J. B. Parise, *Phase Transitions and Compressibility of NaMgF<sub>3</sub> (Neighborite) in Perovskite- and Post-Perovskite-Related Structures*, Geophys. Res. Lett. **33**, L11305 (2006).
- [18] C. D. Martin, W. A. Crichton, H. Liu, V. Prakapenka, J. Chen, and J. B. Parise, *Rietveld Structure Refinement of Perovskite and Post-Perovskite Phases of NaMgF<sub>3</sub> (Neighborite) at High Pressures*, Am. Mineral. **91**, 1703 (2006).
- [19] J. Hustoft, K. Catalli, S.-H. Shim, A. Kubo, V. B. Prakapenka, and M. Kunz, *Equation of State of NaMgF<sub>3</sub> Postperovskite: Implication for the Seismic Velocity Changes in the D" Region*, Geophys. Res. Lett. **35**, 2 (2008).
- [20] K. Umemoto and R. M. Wentzcovitch, *Potential Ultrahigh Pressure Polymorphs of ABX<sub>3</sub>-Type Compounds*, Phys. Rev. B **74**, 224105 (2006).
- [21] K. Umemoto, R. M. Wentzcovitch, D. J. Weidner, and J. B. Parise, *NaMgF<sub>3</sub>: A Low-Pressure Analog of MgSiO<sub>3</sub>*, Geophys. Res. Lett. **33**, L15304 (2006).
- [22] B. Grocholski, S. H. Shim, and V. B. Prakapenka, *Stability of the MgSiO<sub>3</sub> Analog NaMgF<sub>3</sub> and Its Implication for Mantle Structure in Super-Earths*, Geophys. Res. Lett. **37**, 1 (2010).
- [23] C. Jakymiw, L. Vočadlo, D. P. Dobson, E. Bailey, A. R. Thomson, J. P. Brodholt, I. G. Wood, and A. Lindsay-Scott, *The Phase Diagrams of KCaF<sub>3</sub> and NaMgF<sub>3</sub> by Ab Initio Simulations*, Phys. Chem. Miner. **45**, 311 (2018).
- [24] R. Dutta, E. Greenberg, V. B. Prakapenka, and T. S. Duffy, *Phase Transitions beyond Post-Perovskite in NaMgF<sub>3</sub> to 160 GPa*, Proc. Natl. Acad. Sci. **116**, 19324 (2019).
- [25] K. Umemoto and R. M. Wentzcovitch, *Ab Initio Exploration of Post-PPV Transitions in Low-Pressure Analogs of MgSiO<sub>3</sub>*, Phys. Rev. Mater. **3**, 123601 (2019).
- [26] J. P. Poirier, J. Peyronneau, J. Y. Gesland, and G. Brebec, *Viscosity and Conductivity of the Lower Mantle; an Experimental Study on a MgSiO<sub>3</sub> Perovskite Analogue, KZnF<sub>3</sub>*, Phys. Earth Planet. Inter. **32**, 273 (1983).
- [27] F. Aguado, F. Rodríguez, S. Hirai, J. N. Walsh, A. Lennie, and S. A. T. Redfern, *High-Pressure Behaviour of KMF<sub>3</sub> Perovskites*, High Press. Res. **28**, 539 (2008).
- [28] G. Vaitheeswaran, V. Kanchana, X. Zhang, Y. Ma, A. Svane, and N. E. Christensen, *Calculated High-Pressure Structural Properties, Lattice Dynamics and Quasi Particle Band Structures of Perovskite Fluorides KZnF<sub>3</sub>, CsCaF<sub>3</sub> and BaLiF<sub>3</sub>*, J. Phys. Condens. Matter **28**, 315403 (2016).

- [29] K. S. Knight, C. L. Bull, and P. McIntyre, *Low Temperature, High Pressure Thermo-Physical and Crystallographic Properties of  $KZnF_3$  Perovskite*, Mater. Chem. Phys. **199**, 393 (2017).
- [30] K. Hirose, K. Kawamura, Y. Ohishi, S. Tateno, and N. Sata, *Stability and Equation of State of  $MgGeO_3$  Post-Perovskite Phase*, Am. Mineral. **90**, 262 (2005).
- [31] G. Shukla, M. Topsakal, and R. M. Wentzcovitch, *Spin Crossovers in Iron-Bearing  $MgSiO_3$  and  $MgGeO_3$ : Their Influence on the Post-Perovskite Transition*, Phys. Earth Planet. Inter. **249**, 11 (2015).
- [32] C. V. Stan, R. Dutta, R. J. Cava, V. B. Prakapenka, and T. S. Duffy, *High-Pressure Study of Perovskites and Postperovskites in the  $(Mg,Fe)GeO_3$  System*, Inorg. Chem. **56**, 8026 (2017).
- [33] R. Dutta, C. E. White, E. Greenberg, V. B. Prakapenka, and T. S. Duffy, *Equation of State of the  $\alpha$ - $PbO_2$  and Pa-3-Type Phases of  $GeO_2$  to 120 GPa*, Phys. Rev. B **98**, 144106 (2018).
- [34] C. Xu, B. Xu, Y. Yang, H. Dong, A. R. Oganov, S. Wang, W. Duan, B. Gu, and L. Bellaiche, *Prediction of a Stable Post-Post-Perovskite Structure from First Principles*, Phys. Rev. B **91**, 020101 (2015).
- [35] K. Umemoto, R. M. Wentzcovitch, and P. B. Allen, *Dissociation of  $MgSiO_3$  in the Cores of Gas Giants and Terrestrial Exoplanets*, Science (80-. ). **311**, 983 (2006).
- [36] K. Umemoto and R. M. Wentzcovitch, *Two-Stage Dissociation in  $MgSiO_3$  Post-Perovskite*, Earth Planet. Sci. Lett. **311**, 225 (2011).
- [37] K. Umemoto, R. M. Wentzcovitch, S. Wu, M. Ji, C.-Z. Wang, and K.-M. Ho, *Phase Transitions in  $MgSiO_3$  Post-Perovskite in Super-Earth Mantles*, Earth Planet. Sci. Lett. **478**, 40 (2017).
- [38] J. P. Perdew, A. Ruzsinszky, G. I. Csonka, O. A. Vydrov, G. E. Scuseria, L. A. Constantin, X. Zhou, and K. Burke, *Restoring the Density-Gradient Expansion for Exchange in Solids and Surfaces*, Phys. Rev. Lett. **100**, 136406 (2008).
- [39] S. J. Clark, M. D. Segall, C. J. Pickard, P. J. Hasnip, M. I. J. Probert, K. Refson, and M. C. Payne, *First Principles Methods Using CASTEP*, Zeitschrift Fur Krist. - Cryst. Mater. **220**, 567 (2005).
- [40] See Supplemental Material at <http://link.aps.org/supplemental/10.1103/PhysRevMaterials.5.113602> for comparison between theory and experiment for  $GdFeO_3$ -type  $NaZnF_3$ ; phonon dispersion curves; powder x-ray diffraction patterns; pressure dependence of the volume of Na-Zn-F phases, their simulated

Raman spectrum and structural parameters; comparison between  $\text{Na}_2\text{ZnF}_4$ ,  $\text{Mg}_2\text{SiO}_4$  and  $\text{CdMn}_2\text{O}_4$ .

- [41] H. J. Monkhorst and J. D. Pack, *Special Points for Brillouin-Zone Integrations*, Phys. Rev. B **13**, 5188 (1976).
- [42] B. G. Pfrommer, M. Côté, S. G. Louie, and M. L. Cohen, *Relaxation of Crystals with the Quasi-Newton Method*, J. Comput. Phys. **131**, 233 (1997).
- [43] P. Avery, C. Toher, S. Curtarolo, and E. Zurek, *XtalOpt Version R12: An Open-Source Evolutionary Algorithm for Crystal Structure Prediction*, Comput. Phys. Commun. **237**, 274 (2019).
- [44] G. Kresse and J. Furthmüller, *Efficient Iterative Schemes for Ab Initio Total-Energy Calculations Using a Plane-Wave Basis Set*, Phys. Rev. B **54**, 11169 (1996).
- [45] G. Kresse and D. Joubert, *From Ultrasoft Pseudopotentials to the Projector Augmented-Wave Method*, Phys. Rev. B **59**, 1758 (1999).
- [46] K. Refson, P. R. Tulip, and S. J. Clark, *Variational Density-Functional Perturbation Theory for Dielectrics and Lattice Dynamics*, Phys. Rev. B **73**, 155114 (2006).
- [47] K. Momma and F. Izumi, *VESTA 3 for Three-Dimensional Visualization of Crystal, Volumetric and Morphology Data*, J. Appl. Crystallogr. **44**, 1272 (2011).
- [48] H. T. Stokes and D. M. Hatch, *FINDSYM: Program for Identifying the Space-Group Symmetry of a Crystal*, J. Appl. Crystallogr. **38**, 237 (2005).
- [49] T. Yagi, T. Suzuki, and S.-I. Akimoto, *New High-Pressure Polymorphs in Sodium Halides*, J. Phys. Chem. Solids **44**, 135 (1983).
- [50] A. Perakis, D. Lampakis, Y. C. Boulmetis, and C. Raptis, *High-Pressure Raman Study of the Ferroelastic Rutile-to- $\text{CaCl}_2$  Phase Transition in  $\text{ZnF}_2$* , Phys. Rev. B **72**, 144108 (2005).
- [51] K. Kusaba and T. Kikegawa, *In Situ X-Ray Observation of Phase Transitions in  $\text{ZnF}_2$  under High Pressure and High Temperature*, Solid State Commun. **145**, 279 (2008).
- [52] D. Kurzydłowski, A. Oleksiak, S. B. Pillai, and P. K. Jha, *High-Pressure Phase Transitions of Zinc Difluoride up to 55 GPa*, Inorg. Chem. **59**, 2584 (2020).
- [53] S. Ma, S. Li, T. Gao, and B. Ao, *Pressure-Stabilized Zinc Trifluoride*, J. Phys. Chem. Lett. **11**, 2854 (2020).

- [54] S. Yakovlev, M. Avdeev, and M. Mezouar, *High-Pressure Structural Behavior and Equation of State of NaZnF<sub>3</sub>*, *J. Solid State Chem.* **182**, 1545 (2009).
- [55] M. Akaogi, Y. Shirako, H. Kojitani, T. Nagakari, H. Yusa, and K. Yamaura, *High-Pressure Transitions in NaZnF<sub>3</sub> and NaMnF<sub>3</sub> Perovskites, and Crystal-Chemical Characteristics of Perovskite–Postperovskite Transitions in ABX<sub>3</sub> Fluorides and Oxides*, *Phys. Earth Planet. Inter.* **228**, 160 (2014).
- [56] H. Cheng, A.-J. Mao, X.-R. Cheng, H. Tian, X.-L. Dou, S.-M. Yang, and X. Kuang, *Hydrostatic Pressure Induced Structural Phase Transition and Mechanical Properties of Fluoroperovskite*, *J. Phys. Condens. Matter* **31**, 505406 (2019).
- [57] I. Sanchez-Movellan, J. A. Aramburu, and M. Moreno, *Local Structure and Excitations in Systems with CuF<sub>6</sub><sup>4-</sup> Units: Lack of Jahn-Teller Effect in the Low Symmetry Compound Na<sub>2</sub>CuF<sub>4</sub>*, *Phys. Chem. Chem. Phys.* **22**, 7875 (2020).
- [58] D. Zagorac, H. Müller, S. Ruehl, J. Zagorac, and S. Rehme, *Recent Developments in the Inorganic Crystal Structure Database: Theoretical Crystal Structure Data and Related Features*, *J. Appl. Crystallogr.* **52**, 918 (2019).
- [59] R. Kanno, Y. Takeda, K. Murata, and O. Yamamoto, *Crystal Structure of Double Chlorides, Na<sub>2</sub>MCl<sub>4</sub> (M=Mg, Cr, Cd): Correlation with Ionic Conductivity*, *Solid State Ionics* **39**, 233 (1990).
- [60] D. Kurzydłowski, M. Derzsi, A. Budzianowski, Z. Jagličić, W. Koźmiński, Z. Mazej, and W. Grochala, *Polymorphism of Fluoroargentates(II): Facile Collapse of a Layered Network of  $\alpha$ -K<sub>2</sub>AgF<sub>4</sub> Due to the Insufficient Size of the Potassium Cation*, *Eur. J. Inorg. Chem.* **2010**, 2919 (2010).
- [61] D. Babel and M. Otto, *Die Jahn-Teller-Verzerrung in Den Kristallstrukturen Der Dinatrium-Tetrafluorometallate Na<sub>2</sub>CuF<sub>4</sub> Und Na<sub>2</sub>CrF<sub>4</sub>*, *Zeitschrift Für Naturforsch. B* **44**, 715 (1989).
- [62] D. Kurzydłowski, M. Derzsi, Z. Mazej, and W. Grochala, *Crystal, Electronic, and Magnetic Structures of M<sub>2</sub>AgF<sub>4</sub> (M = Na–Cs) Phases as Viewed from the DFT+U Method*, *Dalt. Trans.* **45**, 16255 (2016).
- [63] A. P. B. Sinha, N. R. Sanjana, and A. B. Biswas, *The Crystal Structure of Cadmium Manganite, Cd[Mn<sub>2</sub>]O<sub>4</sub>*, *Zeitschrift Für Krist.* **109**, 410 (1957).
- [64] D. Kurzydłowski, M. Derzsi, E. Zurek, and W. Grochala, *Fluorides of Silver Under Large*

*Compression*, Chem. – A Eur. J. **27**, 5536 (2021).

- [65] S. Q. Wu, M. Ji, C. Z. Wang, M. C. Nguyen, X. Zhao, K. Umemoto, R. M. Wentzcovitch, and K. M. Ho, *An Adaptive Genetic Algorithm for Crystal Structure Prediction*, J. Phys. Condens. Matter **26**, 1 (2014).
- [66] H. Niu, A. R. Oganov, X.-Q. Chen, and D. Li, *Prediction of Novel Stable Compounds in the Mg-Si-O System under Exoplanet Pressures*, Sci. Rep. **5**, 18347 (2016).
- [67] T. Qin, Q. Zhang, R. M. Wentzcovitch, and K. Umemoto, *Qha: A Python Package for Quasiharmonic Free Energy Calculation for Multi-Configuration Systems*, Comput. Phys. Commun. **237**, 199 (2019).
- [68] J.-B. Wu, X.-L. Cheng, H. Zhang, and Z.-W. Xiong, *First-Principles Study of Structural, Electronic and Optical Properties of ZnF<sub>2</sub>*, Chinese Phys. B **23**, 077102 (2014).
- [69] P. Xiao, J.-G. Cheng, J.-S. Zhou, J. B. Goodenough, and G. Henkelman, *Mechanism of the CaIrO<sub>3</sub> Post-Perovskite Phase Transition under Pressure*, Phys. Rev. B **88**, 144102 (2013).
- [70] K. Yamada, *Structural Phase Transition of the Two-Dimensional Fluoride Ion Conductor KSn<sub>2</sub>F<sub>5</sub> Studied by X-Ray Diffraction*, Solid State Ionics **167**, 301 (2004).
- [71] P. Berastegui, S. Hull, and S. G. Eriksson, *A High Temperature Superionic Phase of CsSn<sub>2</sub>F<sub>5</sub>*, J. Solid State Chem. **183**, 373 (2010).
- [72] Y. Le Fur and S. Aléonard, *Structure Du Pentafluorodibéryllate CsBe<sub>2</sub>F<sub>5</sub>*, Acta Crystallogr. Sect. B Struct. Crystallogr. Cryst. Chem. **28**, 2115 (1972).
- [73] B. Bachmann and B. G. Müller, *Über Komplexe Fluoride Des Zweiwertigen Palladiums*, Zeitschrift Für Anorg. Und Allg. Chemie **616**, 7 (1992).
- [74] N. Ruchaud, J. Grannec, A. Tressaud, and G. Ferey, *Magnetic Structure of CsPd<sub>2</sub>F<sub>5</sub>*, Zeitschrift Für Anorg. Und Allg. Chemie **621**, 1958 (1995).
- [75] V. Kaiser and D. Babel, *Strukturen Caesiumhaltiger Fluoride. IX. CsCu<sub>2</sub>F<sub>5</sub>, Eine Verbindung Mit Den Koordinationszahlen 4, 5 Und 6 Für Kupfer(II)*, Zeitschrift Für Anorg. Und Allg. Chemie **595**, 139 (1991).
- [76] D. Y. Aydın, M. Gürü, D. Ipek, and D. Özyürek, *Synthesis and Characterization of Zinc Fluoroborate from Zinc Fluoride and Boron by Mechanochemical Reaction*, Arab. J. Sci. Eng. **42**, 4409 (2017).

- [77] H. Yusa, Y. Shirako, M. Akaogi, H. Kojitani, N. Hirao, Y. Ohishi, and T. Kikegawa, *Perovskite-to-Postperovskite Transitions in  $\text{NaNiF}_3$  and  $\text{NaCoF}_3$  and Disproportionation of  $\text{NaCoF}_3$  Postperovskite under High Pressure and High Temperature*, *Inorg. Chem.* **51**, 6559 (2012).